Physics Letters B 761 (2016) 125–130

Contents lists available at ScienceDirect

Physics Letters B

www.elsevier.com/locate/physletb

Fission fragments mass distributions of nuclei populated by the multinucleon transfer channels of the $^{18}O + ^{232}Th$ reaction

R. Léguillon [a], K. Nishio [a,*], K. Hirose [a], H. Makii [a], I. Nishinaka [a], R. Orlandi [a], K. Tsukada [a], J. Smallcombe [a,b], S. Chiba [c], Y. Aritomo [d], T. Ohtsuki [e], R. Tatsuzawa [f], N. Takaki [f], N. Tamura [g], S. Goto [g], I. Tsekhanovich [h], C.M. Petrache [i], A.N. Andreyev [j,a]

[a] Advanced Science Research Center, Japan Atomic Energy Agency (JAEA), Tokai, Ibaraki 319-1195, Japan
[b] TRIUMF, Vancouver, British Columbia V6T 2A3, Canada
[c] Laboratory for Advanced Nuclear Energy, Institute for Innovative Research, Tokyo Institute of Technology, N1-9, 2-12-1 Ookayama, Meguro, Tokyo 152-8550, Japan
[d] Faculty of Science and Engineering, Kindai University, Higashi-Osaka, 577-8502, Japan
[e] Research Reactor Institute, Kyoto University, Kumatori-cho, Sennangun, Osaka 590-0494, Japan
[f] Graduate School of Engineering, Tokyo City University, Tokyo 158-8557, Japan
[g] Graduate School of Science and Technology, Niigata University, Niigata 950-2181, Japan
[h] University of Bordeaux, 351 Cours de la Libration, 33405 Talence Cedex, France
[i] Centre des Sciences Nucléaire et des Sciences de la Matière, Université Paris-Saclay, CNRS/IN2P3, 91406 Orsay, France
[j] Department of Physics, University of York, Heslington, York, YO10 5DD, United Kingdom

ARTICLE INFO

Article history:
Received 3 May 2016
Received in revised form 18 June 2016
Accepted 5 August 2016
Available online 9 August 2016
Editor: V. Metag

Keywords:
Fission
Multinucleon transfer reaction
Fission fragment mass distribution
$^{231-234}$Th
$^{232-236}$Pa
$^{234-238}$U

ABSTRACT

It is shown that the multinucleon transfer reactions is a powerful tool to study fission of exotic neutron-rich actinide nuclei, which cannot be accessed by particle-capture or heavy-ion fusion reactions. In this work, multinucleon transfer channels of the $^{18}O + ^{232}Th$ reaction are used to study fission of fourteen nuclei ^{231,232,233,234}Th, ^{232,233,234,235,236}Pa, and ^{234,235,236,237,238}U. Identification of fissioning nuclei and of their excitation energy is performed on an event-by-event basis, through the measurement of outgoing ejectile particle in coincidence with fission fragments. Fission fragment mass distributions are measured for each transfer channel, in selected bins of excitation energy. In particular, the mass distributions of ^{231,234}Th and ^{234,235,236}Pa are measured for the first time. Predominantly asymmetric fission is observed at low excitation energies for all studied cases, with a gradual increase of the symmetric mode towards higher excitation energy. The experimental distributions are found to be in general agreement with predictions of the fluctuation–dissipation model.

1. Introduction

Induced nuclear fission is a unique decay process which may be described by the interplay of macroscopic (collective) and microscopic (single particle) degrees of freedom in a nucleus [1]. Such a description of the fission process allows for studies of nuclear shell structures, nuclear viscosity and their excitation energy dependence at extreme values of deformation. In particular, fission fragment (FF) mass distributions and their sensitivity to the excitation energy and isospin provide a deep insight into the mechanism of the process of fission (see e.g. [2,3]).

Since the discovery of fission more than 75 years ago [4], fission process was intensively studied in capture reactions with light particles (e.g. neutrons, protons, electrons) and gamma rays, as well as with spontaneously fissioning nuclei [5]. With the development of more versatile accelerators, complete-fusion reactions with heavy ions and also few-nucleon direct transfer reactions of e.g. (d,pf), (^{3}He,pf) or (^{6}Li,df) and similar types started to be exploited. Often, such studies concentrated mostly on the measurements of fission probabilities and their excitation energy dependence, see e.g. [6–13] and a review of experiments on the so-called 'surrogate' fission given in [14]. One of the first examples of fission fragments mass distribution (FFMD) measurements via the direct few-nucleon transfer was reported in [15] for the isotopes ^{227,228}Ac, studied with the ^{226}Ra(^{3}He,df) and ^{226}Ra(^{3}He,pf) reactions, respectively. The FFMD of the ^{239}Pu(d,pf) reaction via the superdeformed

* Corresponding author.
E-mail address: nishio.katsuhisa@jaea.go.jp (K. Nishio).

http://dx.doi.org/10.1016/j.physletb.2016.08.010

β vibrational resonance was studied [16]. As a general rule, such studies mostly rely on the use of stable or long-lived primordial nuclides as a target, such as isotopes of Th, U and some of the long-lived heavier transactinides, some of the latter could also be obtained via the neutron activation in high-flux reactors. An extreme case of the latter approach is the spontaneous fission study of ^{259}Fm [17], produced in the ^{257}Fm(t,p)^{259}Fm $\rightarrow$ (SF) reaction. Overall, the region of nuclei accessible for early fission studies was limited to nuclei lying close to the beta-stability line or to very neutron-deficient isotopes produced in complete-fusion reactions.

Recently, several different approaches to perform FFMD measurements in the very neutron-deficient mercury-to-thorium nuclei were demonstrated in the reactions with radioactive beams. In particular, at ISOLDE, by using beta-delayed fission, fission properties of the very neutron-deficient ^{178,180}Hg ($N/Z \sim 1.25$), ^{194,196}Po and of ^{202}Rn were investigated [18–20]. At FRS@GSI, by using low-energy Coulex-induced fission of relativistic RIBs in inverse kinematics, comprehensive fission studies were performed for several tens of nuclei in the neutron-deficient Ac–U region [21]. The recent SOFIA experiment at GSI also followed the same approach but with a much improved technique [22]. Despite a wealth of new information produced by these methods, presently they can be applied to nuclei only up to ^{238}Np.

The scope of the present work is to explore the potential of the multinucleon transfer (MNT) reactions to measure FFMDs and their excitation energy dependence for the neutron-rich nuclei, which cannot be accessed by particle-capture and/or heavy-ion fusion reactions. The MNT channels of the ^{238}U + ^{12}C reaction in inverse kinematics were recently used to study fission of excited transactinide nuclei with the help of the large-acceptance magnetic spectrometer VAMOS@GANIL [23–25]. In these experiments, sufficiently-high A and Z resolution for FFs was achieved due to their kinematic boost, allowing the simultaneous measurement of the complete mass- and atomic-number distributions of fission fragments (at least for the light FF groups) using the magnetic spectrometer. For completeness, we also mention a recent nuclear-decay spectroscopy study of fission fragments at the large-aperture magnetic spectrometer PRISMA (LNL, Legnaro, Italy) coupled to the high-resolution Advanced Gamma Tracking Array (AGATA) [26]. In that work, the initial fissioning nuclei in the vicinity of ^{238}U were produced in the near-barrier transfer channels of the ^{136}Xe + ^{238}U reaction. More generally, the use of the MNT reactions has recently attracted considerable attention to produce neutron-rich nuclei in the vicinity of the $N = 126$ shell closure [27] and also neutron-rich super-heavy elements [28,29].

In this Letter, we studied the MNT channels of the reaction ^{18}O + ^{232}Th in direct kinematics to obtain FFMDs and their excitation-energy dependence for fourteen excited isotopes of Th, Pa and U. An obvious advantage of this method is a relatively easy possibility to change the projectile and/or the target nuclei. In particular by using targets of the rarest highly-radioactive neutron-rich isotopes heavier than ^{238}U (e.g. Cm and Cf), nuclei to be studied can be extended to isotopes far heavier than uranium, which cannot be used at the accelerator facilities for the inverse kinematics experiments similar to VAMOS or SOFIA.

2. Experimental methods

An ^{18}O beam of 157.0 MeV was supplied by the JAEA-tandem accelerator at a typical beam intensity of 0.4 pnA. A 148 μg/cm^2 thick ^{232}Th target was prepared by electrodeposition of ^{232}ThO$_2$ on a Ni backing of about 90 μg/cm^2 thickness with a diameter of 5 mm.

For the event-by-event identification of the transfer channel (thus, of the fissioning nucleus) and of respective coincident FFs,

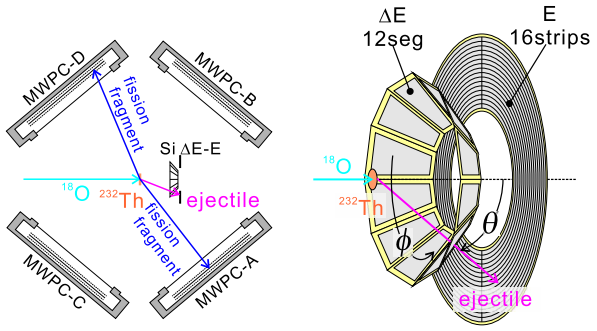

(a) Schematic detection set-up (left) and expanded view of the silicon ΔE–E detector telescope (right). See text for details.

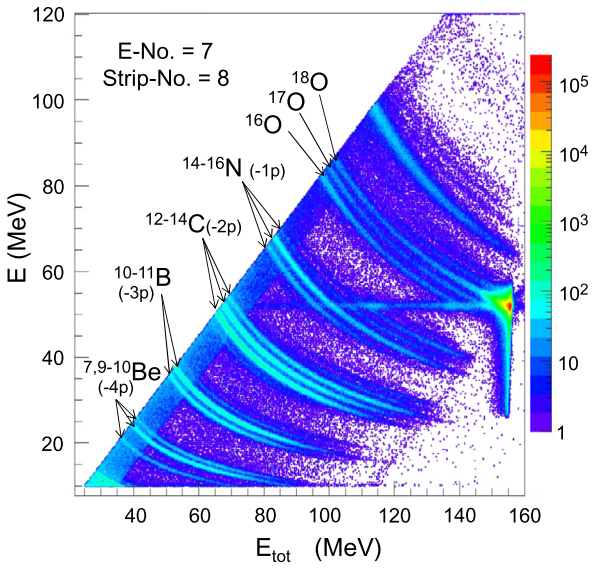

(b) ΔE–E_{tot} spectrum for ejectiles measured by one pair of the ΔE–E detectors. The curves corresponding to different ejectiles are marked with the respective isotopes. The scattered ^{18}O is also seen in the plot.

Fig. 1. (Color online) (a) Experimental setup and (b) identification of the transfer channel using the ΔE–E telescope.

a detection system consisting of a ΔE–E silicon detector telescope and four multiwire proportional chambers (MWPC) were used, see Fig. 1(a). Specific transfer channels were identified by detecting projectile-like (ejectile) nuclei in twelve 75 μm-thick trapezoidal ΔE silicon detectors which were mounted in a cone around the beam axis, each with the azimuthal angle acceptance of $\Delta\varphi = 22.5°$. After passing through the ΔE detector, the ejectiles impinged on the 300 μm-thick annular silicon strip detector (E-detector), divided in 16 annular strips, which allows determination of the scattering angle θ. The inner and outer radius of the detector are 24.0 mm and 48.0 mm, respectively, corresponding to the acceptance angle θ between 16.7° and 31.0° relative to the beam direction.

The energy calibration of the E-detectors was performed by removing two ΔE-detectors so that the elastically-scattered ^{18}O beam could hit the E-detector directly. The well-defined initial beam energy from the tandem and the measured scattering energy $E_{elastic}(\theta)$ (as a function of the scattering angle) were then used to calibrate the strips of the E-detector. Elastic scattering was further used to calibrate the ΔE-detectors, by determining the energy deposition in the ΔE-detector as $E_{elastic}$–E_{res}, where E_{res} is the energy measured in the E-detector after passing through the ΔE-detector. From the peak of elastic scattering in the sum spec-

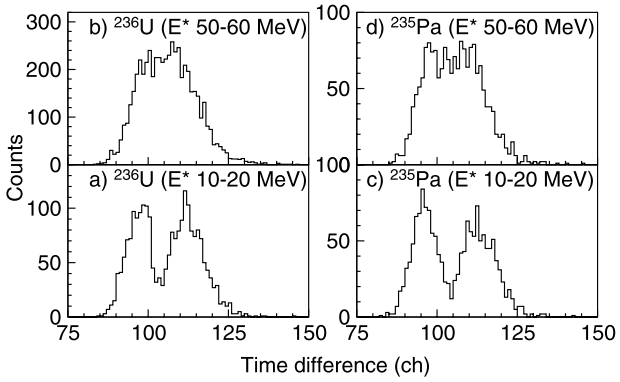

Fig. 2. "Raw" FFs time difference spectra obtained for ^{236}U* (^{14}C detected in the silicon telescope detectors) and ^{235}Pa* (^{15}N detected) fissioning nuclei at lower and higher excitation energies.

trum $E_{\rm tot} = \Delta E + E_{\rm res}$, the energy resolution was obtained to be 1.0 MeV (FWHM), which also determines the precision for the excitation energies deduced in our study (see also in the follow-up text).

Fig. 1(b) shows the ΔE–$E_{\rm tot}$ spectrum for ejectiles, where the parabolic lines correspond to different transfer channels, including a clear separation of specific isotopes. Isotopic assignment was done in respect of the elastically-scattered peak of ^{18}O and the missing line of ^{8}Be. It was further confirmed with the energy-loss calculation using the program SRIM [30]. The identification of the ^{12}C line was also checked by accelerating a ^{12}C beam and measuring the elastic peak. The data from ΔE–E spectra were also used to deduce the excitation energy of the respective fissioning nuclei, which were determined from reaction Q-value [31] and the measured (angle-dependent) ejectile energies ΔE and $E_{\rm tot}$. In this procedure we assumed that no excitation energy is given to the ejectile, thus the excitation energies quoted in the paper should be considered as upper limits only. Furthermore, though the precision of the deduced excitation energies is $\sim$ 1 MeV (see above), we bin the events into the ranges of excitation energy $\sim$ 10 MeV wide, as a compromise between the observed statistics within each bin and reasonably maintaining narrow bin sizes.

The coincident FFs resulting from the fission of excited nuclei (after the MNT) are detected by four 200 $\times$ 200 mm^2 position-sensitive MWPC, see in Fig. 1(a). Operation conditions are described in [32]. The distance between the target and the center of the cathode was 224 mm, and each MWPC covers a solid angle of 0.67 sr. The positions of FFs's incidence on the MWPC were determined with a position resolution of 4.0 mm. FF time differences, ΔT, between two coincident MWPCs were measure to determine the masses of both fragments.

Fig. 2 shows examples of 'raw' FF ΔT spectra obtained for two transfer channels ^{18}O + ^{232}Th $\rightarrow$ ^{14}C + ^{236}U* and ^{18}O + ^{232}Th $\rightarrow$ ^{15}N + ^{235}Pa*, summed over all ΔE–E detectors. To demonstrate the evolution of the ΔT spectra as a function of the excitation energy, the data are shown in the low- ($E^* = 10$–20 MeV) and higher-excitation ($E^* = 50$–60 MeV) energy ranges. It is seen from Fig. 2 that the spectra (a) and (c), obtained at low excitation energies, provide a clear signature of predominantly mass-asymmetric fission. At high excitation energies (spectra (b) and (d)), both distributions change to more symmetric shapes but still indicate a component of asymmetric fission.

3. Results

FFs masses were determined event-by-event from the kinematic analysis, whereby the measured ΔT values and incident positions

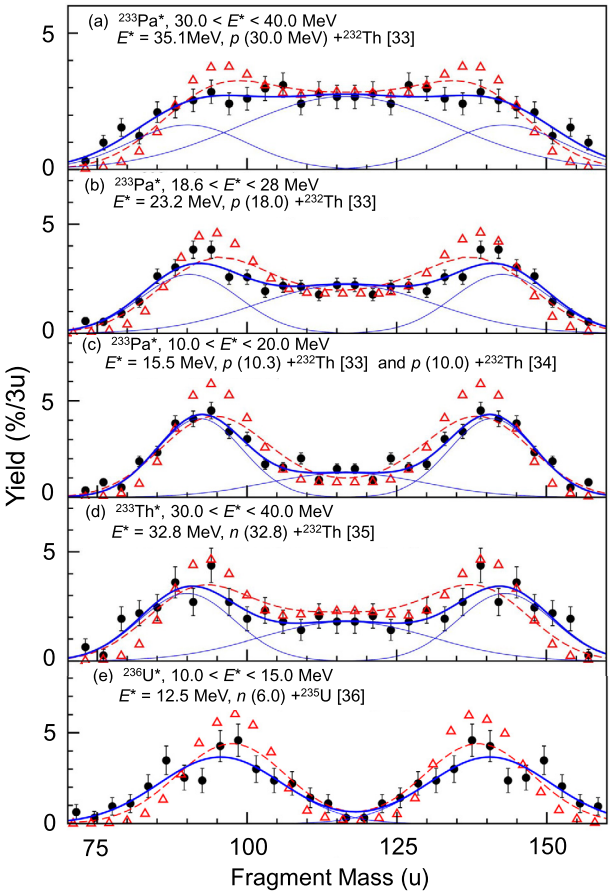

Fig. 3. (Color online) Experimental FFMDs (closed circles with error bars) and literature data (open triangles) for ^{233}Pa* (panels (a)–(c), different ranges of excitation energy), (d) ^{233}Th* and (e) ^{236}U*. Excitation energy range is shown for our data, while specific values of E^* at which the data were measured, are shown for the literature data. The red dashed curves show the literature data [33–36] smeared out with the present mass resolution. The blue thick line shows the fit with symmetric and asymmetric modes, for which the respective Gaussian functions are given by thin blue lines. The sum of the yield of the FFMD is normalized to 200.

of both FFs were used. The momentum of the target-like fissioning recoil nucleus is determined by the measured momentum of ejectile under the assumption of a binary reaction process. To validate the calibration procedure, Fig. 3 compares a selection of deduced FFMD's (full black circles with the error bars) with the literature data (red open triangles) [33–36] for ^{233}Pa*, ^{233}Th* and ^{236}U*, obtained at comparable excitation energies. We note that the present FFMDs are typically broader than the literature data, which is due to limited mass resolution, mainly originating from a relatively thick target used in our study. The experimental mass resolution of $\sigma_{\rm m} = 6.5$ u was determined by comparing the measured FFMD for ^{233}Pa* at average excitation energy of $E^* \sim 15$ MeV with the literature data taken at comparable excitation energies in the p + ^{232}Th to ^{233}Pa* reaction [33,34]. For the sake of comparison with our data, the literature data were artificially broadened by the experimental resolution and are shown as red dashed curves, which are in a reasonable agreement with our data, thereby confirming the validity of the whole method.

Fig. 3 also shows the benchmarking of the fitting procedure used to extract the most probable masses of the light and heavy peaks of the FFMDs. Following the procedure of [33] (in particular their Figs. 9–11), the fitting was performed by a combination of two main fission modes, mass-symmetric Standard (S) and asymmetric Standard-2 (S2) in [33], the respective Gaussian functions

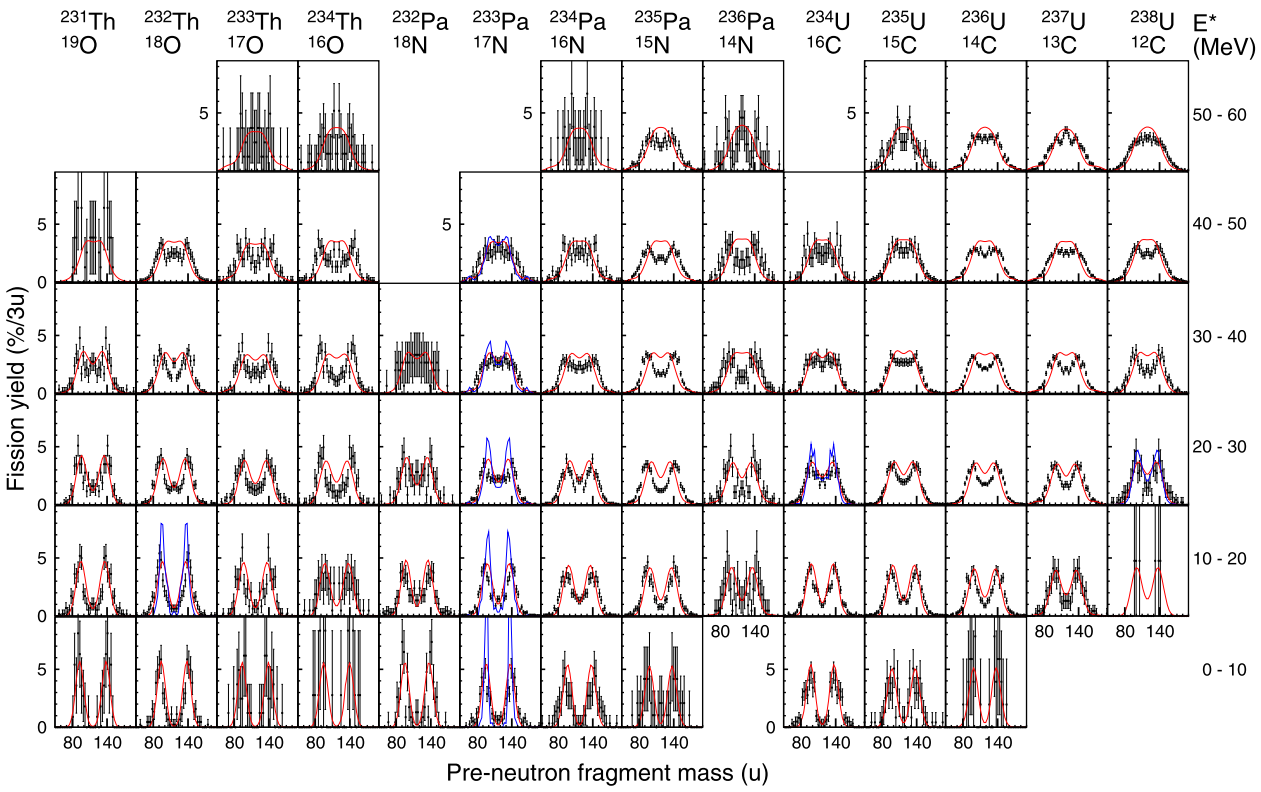

Fig. 4. (Color online) FFMDs obtained in the multinucleon transfer channels of the reaction $^{18}O + ^{232}Th$ (data points with error bars). The fissioning nucleus and the corresponding ejectile are indicated on the top of the plot. The data are shown for sequential 10 MeV excitation-energy E^* intervals, indicated on the right side. The red curves are the results of Langevin calculations (see text) after broadening with the experimental resolution. Several examples of the original FFMD calculations are shown in blue.

are shown by the thin blue lines with the final total fit given by a thick blue line. The fits demonstrate that quite a fair description of our data is obtained for all five cases in the figure. In particular, we stress a reasonable description of the FFMDs of $^{233}Pa^*$ at three excitation energies, which shows a gradual increase of the symmetric component in the fitting function, in agreement with more precise data shown in e.g. [33]. We note that fitting in [33] also included two extra modes, Standard-1 (S1) of moderate mass-asymmetry and Standard-3 (S3) of super mass-asymmetry. However, these modes contribute less than $\sim 10\%$ and $\sim 0.5\%$, respectively, to the total yield (see Figs. 9, 10 of [33]) and their weight is smaller than the uncertainty of our measurement. Therefore, their omission from our fits will not change the main conclusions of the present work.

Fig. 4 summarizes the FFMDs obtained in this experiment for nuclei of $^{231-234}Th^*$, $^{232-236}Pa^*$ and $^{234-238}U^*$, for excitation energy bins of 10 MeV. FFMDs of the $^{231,234}Th^*$, $^{234,235,236}Pa^*$ nuclei were obtained for the first time. For the other nuclei, the known FFMD data were systematically extended to excitation energies as high as 60 MeV. It follows from Fig. 4 that mass-asymmetric fission dominates at low excitation energies for all measured nuclei. The yield in the mass-symmetric fission region increases with excitation energy (see also Fig. 3 for a zoom-in view for $^{233}Pa^*$) and the double-humped shapes tend to become structureless due to weakening of shells responsible for asymmetric fission. It is also interesting to note that the measured spectra seem to reveal larger peak-to-valley ratio in the FFMDs for nuclei with larger isospin values, as seen for the most neutron-rich isotopes of the same element, considered at the same excitation energy (see, for instance, FFMDs for $E^* = 20$–40 MeV). This might be explained by the growing influence of the magic ^{132}Sn nucleus on the mass division, which is expected for lower mismatches in the N/Z-ratios between ^{132}Sn and the fissioning compound nucleus.

Concerning the results presented in Fig. 4 it should be stressed that initial excitation energy of a fissioning system, E^*, can be reduced by evaporation of neutrons prior to fission, especially when the excitation energy is high. As shown in [37], the pre-scission neutron multiplicities M_{pre} are expected to linearly increase with E^* from a threshold for neutron-emission. Based on the parameters best fitted for isotopes of Pa and U elements, the M_{pre} is estimated to evolve as 0.6, 1.2 and 1.8, for the initial excitation energy values of $E^* = 40$, 50, and 60 MeV. Taking into account average of the neutron binding energy for nuclei shown in Fig. 4 as 5.8 MeV [38] as well as mean energy of evaporated neutrons obtained from the PACE2 code [39] (for example ~ 1.9 MeV at $E^* = 50$ MeV), the neutron emission leads to lowering the mean excitation energy at fission by 4.5, 9.2, and 14 MeV, at $E^* = 40$, 50 and 60 MeV, respectively.

4. Discussion

From the two-fission mode fitting procedure, the most probable mass values for the light and heavy FFs groups, $\langle A_L \rangle$ and $\langle A_H \rangle$ were extracted. The obtained values are shown in Fig. 5 by closed circles with error bars, together with the literature values for 'benchmark' isotopes $^{233}Th^*$, $^{233}Pa^*$ and $^{236}U^*$ (open triangles). Despite relatively large experimental uncertainties, one notices that, on average for the low excitation of $E^* < 20$ MeV, the fitted position of the heavy peak in all studied systems remains constant at $\langle A_H \rangle = 140 \sim 142$, while the light-fragment peak gradually increases from $\langle A_L \rangle \sim 90$ to ~ 97 when the system transit from the lightest to the heaviest nuclei. An interesting finding in our work is that the location of the light- and heavy peaks are nearly con-

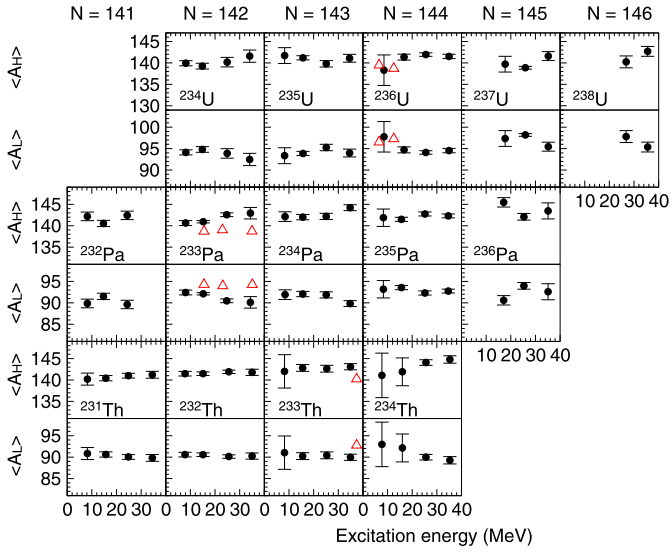

Fig. 5. (Color online) Solid symbols with error bars—the heavy and light FFs masses obtained by a simultaneous fitting the experimental data with symmetric and asymmetric fission modes. For comparison, the previously published data for ^{233}Th* [35], ^{233}Pa* [33], and ^{236}U* [36] were also fitted with the same procedure and the results are shown (open triangle).

stant through the measured excitation energy range, similar to the benchmark data of ^{233}Pa* [33]. Due to lower statistics, we prefer not to rely on the data fits for energies higher than $E^* = 40$ MeV.

The measured FFMDs are compared with calculations based on the fluctuation–dissipation model developed in [40], where description of fission in Langevin equations from the low-excited state were attempted, and a good reproduction of the measured FFMDs for ^{234,236}U* and ^{240}Pu* from $E^* = 20$ MeV was obtained. As described in [40], the nuclear shape and the corresponding energy is calculated by a two-center shell model [41]. The nuclear shape is defined by three parameters (distance between two potential centers, deformation of fragments, and mass-asymmetry), and the corresponding energy is given by a sum of the liquid-drop energy $V_{\rm LD}$ and the shell correction energy $V_{\rm shell}$. The latter term is represented as $V_{\rm shell}(0)\exp(-E^*/E_{\rm d})$ using the shell correction energy at the zero temperature $V_{\rm shell}(0)$ and shell damping parameter $E_{\rm d}$, where $E_{\rm d} = 20$ MeV was chosen as in [40]. For simplicity, it was assumed that the total excitation energy of the system after multinucleon transfer reactions is given to the excitation energy (E^*) of the fissioning nucleus.

It was noticed that the calculated FFMDs have typically a rather narrow distribution in the region of $E^* < 20$ MeV, see a few examples of the original calculations shown in blue in Fig. 4. Therefore the original theoretical curves were broadened with the experimental resolution (cf. a similar procedure in respect of Fig. 3) The resulting broadened theoretical FFMDs are shown by the red solid curves in Fig. 4. One can see that the calculated FFMDs reproduce reasonably well both the global shape of the experimental distributions and also the positions of the light and heavy-fragment peaks for most of studied nuclides, at the excitation energies below ~ 30 MeV. This demonstrates the reasonable treatment of the shell correction energy at these excitation energies, and confirms the validity of the shell-damping energy of $E_{\rm d} = 20$ MeV originally introduced in [42], in contrast to a recently suggested value of $E_{\rm d} = 60$ MeV [43]. However, some local deviations are recognized, especially at higher excitation energies. For example, calculated spectra at $E^* = 30$–40 MeV and higher energies show a tendency to favor the symmetric fission mode for most of the studied nuclei, whereas experimentally several nuclei still exhibit a clear mass asymmetry especially for the most neutron-rich isotopes (for example ^{234}Th*, ^{236}Pa*, ^{238}U*). This observation might point out at too rapid shell dumping with growing excitation energy, especially for neutron rich isotopes.

In summary, multinucleon transfer reactions were used to study the FFMDs and their excition energy dependence in fourteen compound nuclei excited up to $E^* = 60$ MeV; the FFMDs of ^{231,234}Th*, ^{234,235,236}Pa* were measured for the first time.

For all studied cases, the shape of the mass distributions was found to be predominantly asymmetric at low excitation energies, with a gradual increase of the symmetric mode towards higher excitations. For a given isotope chain, the asymmetric mode tends to increase with neutron number, which can be interpreted in terms of the growing influence of doubly magic ^{132}Sn, under the hypothesis that the neutron-to-proton ratio of the compound nucleus is preserved in fission fragments. The measured FFMDs were compared with the three-dimensional Langevin calculations, which are found able to describe in most cases both the shape and the excitation energy dependence, at least up to $E^* \sim 30$ MeV.

The present experiment demonstrates that multinucleon transfer reaction is a useful tool to study fission properties of a number of short-lived neutron-rich actinide and transactinide nuclei. Several instrumental developments are however needed to increase the quality of the data, such as the use of thinner targets ($50 \sim 100$ μg/cm^2), to improve on the mass resolutions, and of an array of γ-ray detectors, to measure possible excitation of the ejectile, which in turn will allow for a better determination of the excitation energy of the fissioning nucleus.

Acknowledgements

Special thanks are due to the crew of the JAEA tandem facility for their beam operation. Present study is supported by “Comprehensive study of delayed-neutron yields for accurate evaluation of kinetics of high-burn up reactors” by the Ministry of Education, Culture, Sports, Science and Technology of Japan (MEXT), and by Science and Technology Facilities Council (STFC) of the UK.

References

[1] C. Wagemans (Ed.), Nuclear Fission Process, CRC Press, Boca Raton, FL, 1991.
[2] U. Brosa, S. Grossmann, A. Müller, Phys. Rep. 167 (1990).
[3] Y. Nagame, H. Nakahara, Radiochim. Acta 100 (2012).
[4] O. Hahn, F. Strassmann, Naturewissenschaften 27 (1) (1939) 11.
[5] D.C. Hoffman, Nucl. Phys. A 502 (1989) 21c.
[6] B.B. Back, et al., Phys. Rev. C 9 (1974) 1924.
[7] B.B. Back, et al., Phys. Rev. C 10 (1974) 1948.
[8] M. Petit, et al., Nucl. Phys. A 735 (2004) 345.
[9] G. Kessedjian, et al., Phys. Lett. B 692 (2010) 297.
[10] V.V. Desai, et al., Phys. Rev. C 87 (2013) 034604.
[11] R.O. Hughes, et al., Phys. Rev. C 90 (2014) 014304.
[12] R.J. Casperson, et al., Phys. Rev. C 90 (2010) 034601.
[13] L. Csige, et al., Phys. Rev. C 85 (2012) 054306.
[14] J.E. Escher, et al., Rev. Mod. Phys. 84 (2012) 353.
[15] E. Konecny, H.J. Specht, J. Weber, Phys. Lett. B 45 (1973) 329.
[16] K. Nishio, et al., Phys. Rev. C 67 (2003) 014604.
[17] E.K. Hulet, et al., Phys. Rev. C 21 (1980) 966.
[18] A.N. Andreyev, M. Huyse, P. Van Duppen, Phys. Rev. Lett. 105 (2010) 252502.
[19] A.N. Andreyev, et al., Rev. Mod. Phys. 85 (2013) 1541.
[20] L. Ghys, et al., Phys. Rev. C 90 (2014) 041301(R).
[21] K.-H. Schmidt, et al., Nucl. Phys. A 665 (2000) 221.
[22] G. Boutoux, et al., Phys. Proc. 47 (2013) 166.
[23] M. Caamaño, et al., Phys. Rev. C 88 (2013) 024605.
[24] M. Caamaño, et al., Phys. Rev. C 92 (2015) 034606.
[25] C. Rodríguez-Tajes, et al., Phys. Rev. C 89 (2014) 024614.
[26] A. Vogt, et al., Phys. Rev. C 92 (2015) 024619.
[27] X.Y. Watanabe, et al., Phys. Rev. Lett. 115 (2015) 172503.
[28] V.I. Zagrebaev, W. Greiner, Phys. Rev. C 83 (2011) 044618.
[29] W. Loveland, Eur. Phys. J. A 25 (2005) 233.

[30] J.F. Siegler, http://www.srim.org/.
[31] G. Audi, et al., Chin. Phys. C 36 (2012) 1287;
M. Wang, et al., Chin. Phys. C 36 (2012) 1603.
[32] K. Nishio, et al., Phys. Rev. C 77 (2008) 064607.
[33] S.I. Mulgin, et al., Nucl. Phys. A 824 (2009) 1.
[34] I. Nishinaka, et al., Phys. Rev. C 70 (2004) 014609;
I. Nishinaka, et al., in: Proceedings of the Fourth International Conference on Fission and Properties of Neutron-Rich Nuclei, Sanibel Island, Florida, USA, 11–17 Nov. 2007, World Scientific, 2007, pp. 206–211.
[35] I.V. Ryzhov, et al., Phys. Rev. C 83 (2011) 054603.
[36] Ch. Straede, B. Jørgensen, H.-H. Knitter, Nucl. Phys. A 462 (1987) 85.
[37] D. Hilscher, H. Rossner, Annu. Phys. Fr. 17 (1992) 471.
[38] P. Möller, et al., At. Data Nucl. Data Tables 109–110 (2016) 1.
[39] A. Gavron, et al., Phys. Rev. C 21 (1980) 230.
[40] Y. Aritomo, S. Chiba, Phys. Rev. C 88 (2013) 044614.
[41] K. Sato, et al., Z. Phys. A 288 (1978) 383.
[42] A.N. Ignatyuk, et al., Sov. J. Nucl. Phys. 21 (1975) 255.
[43] J. Randrup, P. Möller, Phys. Rev. C 88 (2013) 064606.